Equilibrium vortex formation in ultrarapidly rotating two-component Bose-Einstein condensates

C.-H. Hsueh,[1] T.-L. Horng,[2] S.-C. Gou,[3] and W. C. Wu[1]
[1]*Department of Physics, National Taiwan Normal University, Taipei 11677, Taiwan*
[2]*Department of Applied Mathematics, Feng Chia University, Taichung 40724, Taiwan*
[3]*Department of Physics, National Changhua University of Education, Changhua 50058, Taiwan*
(Received 22 April 2011; published 5 August 2011)

Equilibrium vortex formation in rotating binary Bose gases with a rotating frequency higher than the harmonic trapping frequency is investigated theoretically. We consider the system being evaporatively cooled to form condensates and a combined numerical scheme is applied to ensure the binary system being in an authentic equilibrium state. To keep the system stable against the large centrifugal force of ultrafast rotation, a quartic trapping potential is added to the existing harmonic part. Using the Thomas-Fermi approximation, a critical rotating frequency Ω_c is derived, which characterizes the structure with or without a central density hole. Vortex structures are studied in detail with rotation frequency both above and below Ω_c and with respect to the miscible, symmetrically separated, and asymmetrically separated phases in their nonrotating ground-state counterparts.

DOI: 10.1103/PhysRevA.84.023610 PACS number(s): 03.75.Lm, 03.75.Mn, 05.30.Jp

I. INTRODUCTION

Quantum coherence has enabled intriguing phenomena, such as quantized vorticity, in Bose-Einstein condensates (BECs). When a trapped condensate is driven to rotate, singly quantized vortices form. In lower rotations, only one or a few vortices will be present at equilibrium [1]. Faster rotation can generate more vortices which are eventually condensed into a lattice [2–5]. Vorticity in a single-component Bose-Einstein Condensate has indeed been observed in a variety of experiments. On the other hand, since the first experiment of two coexisting condensates of two different hyperfine states of ^{87}Rb [6] was realized, BECs in mixtures of trapped quantum gases provide a unique opportunity to study the miscibility of interpenetrating quantum fluid. Several theoretical articles about binary-mixture condensates have expounded that both the interspecies and the intraspecies interactions play an important role in determining the density patterns and phase separation of the condensates [7–12] . In contrast to the Abrikosov vortex-lattice state of a scalar BEC, the vortex states of binary-mixture BECs have various exotic structures due to the variety of interactions [13–15].

Rotating Bose condensates are usually confined in a harmonic trap with cylindrical symmetry around the rotation axis (say, z direction). In these typical cases, there are two limiting regimes depending on the relative size of the rotating frequency Ω_0 and the trapping frequency ω in the xy plane. When $\Omega_0 > \omega$, the system will become unstable due to a strong centrifugal force. In order to analyze the regime of ultrafast rotations with $\Omega_0 > \omega$, one approach is to add a quartic part to the harmonic potential. In this type of system, the trapping force will be always greater than the centrifugal force and consequently the regime $\Omega_0 > \omega$ can be fully explored [16–23]. The current paper attempts to study the equilibrium vortex states of ultrafast-rotating binary condensates confined in a harmonic-plus-quartic potential.

In a single-component ultrarapidly rotating condensate trapped in a harmonic-plus-quartic potential, the system can experience a Mexican-hat-shape effective potential when $\Omega_0 > \omega$. Depending on how Ω_0 is larger than ω, the system can be roughly separated into two regimes: a condensate with or without the central density hole. More exactly, it has been shown in the literature that there exist three distinct phases for the fast-rotating scalar condensate confined in a harmonic-plus-quartic potential. One is the vortex lattice without a hole (VL), the second is the vortex lattice with a hole (VLH), and the third is the giant vortex state (GV) [19,22]. It is interesting to see how the interspecies and intraspecies interactions play the role in the binary-mixture condensates under fast rotation and, in particular, how the above-mentioned phases manifest in these systems.

Due to the complexity of the interactions in the binary system, a standard imaginary-time propagating method for solving the Gross-Pitaevskii equation (GPE) that converges the results for the true equilibrium states may not be easy to find. It has been shown in Ref. [24] that a GPE with a phenomenological damping term can provide efficient numerical machinery for finding the eigenstates of the time-independent GPE. Moreover, a theory called the stochastic Gross-Pitaevskii equation (SGPE) [25–29], which includes the effects of both the damping term and the fluctuations due to the thermal clouds, has been demonstrated to be an efficient way to study the single-component BEC system. It is also anticipated that the SGPE is an alternatively efficient method for studying the dynamic and equilibrium properties of a multicomponent system near absolute zero.

The paper is organized as follows. In Sec. II, we introduce the theory for studying the equilibrium vortex states of a binary-mixture BEC system. To investigate the regime of ultrafast rotation, the system is trapped under a harmonic-plus-quartic potential. Section III is devoted to a detailed discussion of the vortex structures for fast-rotating binary-mixture BECs. A critical rotation frequency Ω_c is derived and both $\Omega < \Omega_c$ and $\Omega > \Omega_c$ regimes are studied. It is shown explicitly that vortex structures of the system do manifest the ground states of their nonrotating counterparts. Section IV is a brief conclusion.

II. METHODOLOGY

We consider rapidly rotating two-component pancake-shape BECs that are parallel to the xy plane and in a cylindrically symmetric potential. Assuming that the excitation

 ©2011 American Physical Society

in the z direction is suppressed, the system can be treated approximately by a two-dimensional theory. In the mean-field approximation, such a quasi-two-component BEC system in a corotating frame with a rotating frequency Ω_0 around the z axis can be described by the time-dependent coupled GPEs:

$$i\hbar\frac{\partial\Psi_j}{\partial t} = \left(\mathcal{L}_{\rm GP}^{(j)} - \mu_j\right)\Psi_j = \left(\mathcal{H}_j + \sum_{k=1,2} U_{jk}\,|\Psi_k|^2 - \mu_j\right)\Psi_j, \qquad (1)$$

where component $j = 1,2$, $\mathcal{L}_{\rm GP}^{(j)}$ is the GP Hamiltonian, μ_j is the chemical potential, and Ψ_j is the macroscopic wave function normalized under $N_j = \int |\Psi_j|^2 dxdy$ with N_j being the particle number. $\mathcal{H}_j \equiv -\hbar^2\nabla^2/(2m_j) + V_j - \Omega_0 L_z$ is the single-particle Hamiltonian with m_j being the atomic mass, $V_j = m_j\omega_j^2 r^2/2 + u_j r^4/4$ is the trapping potential in polar coordinates (r,ϕ), ω_j is the harmonic trapping frequency, u_j is the strength of the quartic potential, and $L_z = -i\hbar\partial/\partial\phi$ is the z component angular momentum operator. The interaction parameter $U_{jk} = 2\pi\hbar^2\tilde{a}_{jk}(m_j^{-1} + m_k^{-1})$, with $\tilde{a}_{jk}(>0)$ being the effective two-dimensional s-wave scattering length between atoms in components j and k.

As mentioned before, the SGPE approach, which includes both the damping and the fluctuations due to thermal clouds, may be an efficient numerical approach by which to obtain accurate ground states of a given time-independent GPE [24–29]. Here we apply a similar SGPE approach to study the vortex states of an ultrafast-rotating two-component BEC system. The coupled SGPEs for the present binary system can be expressed as

$$i\hbar\frac{\partial\Psi_j}{\partial t} = (1 - i\gamma)\left(\mathcal{L}_{\rm GP}^{(j)} - \mu_j\right)\Psi_j + \eta_\gamma, \qquad (2)$$

where $\eta_\gamma = \eta_\gamma(\mathbf{r},t)$ is a complex Gaussian noise considered to arise due to the contact with the thermal modes. The correlation function associated with the noise is given by $\langle\eta_\gamma^*(\mathbf{r},t)\,\eta_\gamma(\mathbf{r}',t')\rangle = 2\hbar k_B T\gamma\delta(\mathbf{r}-\mathbf{r}')\,\delta(t-t')$. The strength of the noise, and hence the damping, is thus proportional to γ. In principle, γ can be calculated *ab initio* in terms of the Keldysh self-energy [25,26]. However, as we are interested only in the properties at equilibrium, we may approximate it as a spatial and temporal constant. Throughout this paper, γ is reasonably taken to be a small number, 0.01. The temperature is set to be 1 nK which is about 10^{-2} or less of the critical temperature of a typical BEC system.

It should be emphasized that Eq. (2) is a somewhat heuristic phenomenological version of coupled SGPEs, since any coupling between the thermal clouds of two different components is not considered explicitly. While this coupling may play some important role in the dynamics, it is expected that it has only a minor effect on the equilibrium properties.

To reduce the number of parameters, we assume that $m_1 = m_2 \equiv m$, $\omega_1 = \omega_2 \equiv \omega$, $u_1 = u_2 \equiv u$, and $N_1 = N_2 \equiv N$. Moreover, for convenience, the computations are carried out in oscillator units. That is, the length, time, and energy are scaled, respectively, in units of $\sqrt{\hbar/m\omega}$, $1/\omega$, and $\hbar\omega$. As a consequence, the coupled SGPEs (2) take the following dimensionless forms:

$$i\frac{\partial\psi_j}{\partial t} = (1 - i\gamma)\left(-\frac{\nabla^2}{2} + \frac{r^2}{2} + \frac{\lambda r^4}{4} + i\Omega\frac{\partial}{\partial\phi} + \sum_{k=1,2} g_{jk}|\psi_k|^2 - \tilde{\mu}_j\right)\psi_j + \tilde{\eta}_\gamma. \qquad (3)$$

Here we have redefined the normalized wave function $\psi_j \equiv \sqrt{\hbar/(m\omega N)}\Psi_j$, the strength of the quartic trap $\lambda \equiv u\hbar/(m^2\omega^3)$, the interaction constants between atoms $g_{jk} \equiv 4\pi N\tilde{a}_{jk}$, the chemical potential $\tilde{\mu}_j \equiv \mu_j/\hbar\omega$, and the noise $\tilde{\eta}_\gamma \equiv \eta_\gamma/\hbar\omega$. In addition, the rotation rate $\Omega \equiv \Omega_0/\omega$. The rotation rate and the quartic trap strength are fixed at $\Omega = 2.5$ and $\lambda = 1$ in our calculation throughout this paper.

In our calculations, the vortex configurations (and the corresponding chemical potentials) are first obtained by solving the norm-preserving imaginary-time propagation of the time-dependent coupled GPEs (1) starting from an arbitrary trial wave function. The propagation continues until the fluctuation in the norm of the wave function becomes smaller than 10^{-5}. To check whether the vortex configurations obtained and converged by the coupled GPEs in imaginary time are indeed at equilibrium, they are substituted into and treated as the initial states of the coupled SGPEs (2). If the initial state was not an equilibrium state, it kept propagating until the damping term vanishing.

Moreover, we have used the method of lines with spatial discretization by the Fourier pseudospectral method to compute Eqs. (1) and (2)) [or Eq. (3)]. The time integration in Eq. (1) is done by the adaptive Runge-Kutta method of orders 2 and 3 (RK23), which is more time efficient due to an adjustable time step. However, the fourth-order Runge-Kutta method (RK4) is used for Eq. (2) [or Eq. (3)], since the thermal noise term η_γ is proportional to $1/\sqrt{dt}$ and is better computed with a fixed time step.

III. RESULTS AND DISCUSSIONS

A. Nonrotating ground states

Solving the nonrotating ($\Omega = 0$) time-dependent coupled GPEs (1) using the imaginary-time propagating method, we have obtained three distinct phases for the ground states of the binary-mixture condensates. Figure 1 shows the phase diagram of the binary-mixture condensates in terms of the relative interaction strengths, $\alpha_2 \equiv \tilde{a}_{22}/\tilde{a}_{11}$ and $\alpha_{12} \equiv \tilde{a}_{12}/\tilde{a}_{11}$. By symmetry, it is sufficient to consider $\alpha_2 \leqslant 1$ only. The nonrotating binary-mixture condensates are phase miscible in region I and phase separated in regions II (asymmetric) and III (symmetric). As shown in Fig. 1, the boundary between phases I and III is linear with $\alpha_{12} = \alpha_2$. This linear boundary is obtained by jointing nine points of $\alpha_2 = 0.2$ to 1 (spaced by 0.1) together with their corresponding α_{12} determined with precision less than 0.01. The quartic trap (λ) has only a minimal effect on the boundary between the miscible and the symmetric separated phases. On the contrary, the boundary between phases II and III is quite λ dependent. Similarly this phase boundary is obtained by jointing nine points: from $\alpha_2 = 0.4$ to 1 (spaced by 0.1) and their corresponding α_{12} determined with precision less than 0.01. For larger λ,

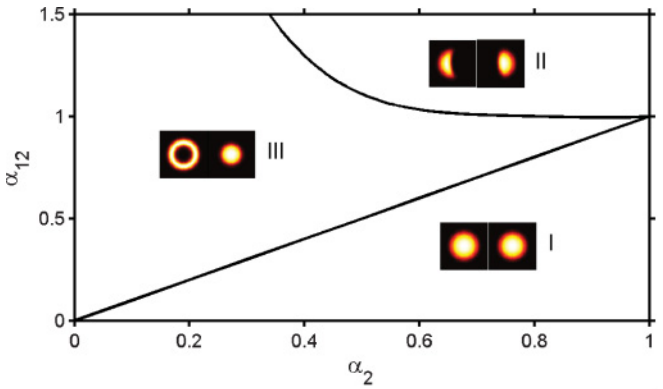

FIG. 1. (Color online) Phase diagram of the nonrotating binary-mixture condensates confined in a harmonic-plus-quartic trap in terms of the relative interaction strengths, $\alpha_2 \equiv \tilde{a}_{22}/\tilde{a}_{11}$ and $\alpha_{12} \equiv \tilde{a}_{12}/\tilde{a}_{11}$. The quartic trap strength is fixed at $\lambda = 1$. Regions I, II, and III correspond to miscible, asymmetrically separated, and symmetrically separated phases, respectively.

due to a relatively stronger confinement which increases the interspecies interaction energy, the two components tend to separate on two sides. Consequently the area of phase II in Fig. 1 will expand as λ increases. This allows a larger space for studying the asymmetric phase-separated regime for fast-rotating binary-mixture condensates. The two boundaries intersect at $(\alpha_2,\alpha_{12}) = (1,1)$ which is called the *isotropic* point. We study the vortex structures in all three phases and in particular at the isotropic point.

B. Critical rotation rate Ω_c

Before discussing the equilibrium vortex formations of fast-rotating binary-mixture condensates, it is useful to identify a critical rotation rate Ω_c which characterizes the states of ultrafast-rotating condensates trapped in a harmonic-plus-quartic potential. In the one-component system, there is only one interaction constant $g \equiv 4\pi N\tilde{a}$, and when $g \gg 1$ the system is in the so-called Thomas-Fermi (TF) regime. As the single-particle GP Hamiltonian under rotation can be written as $\mathcal{L}_{\rm GP} = -1/2(\nabla - i\Omega \times \mathbf{r})^2 + V_{\rm eff}(r) + g|\psi|^2$ with the effective trapping potential $V_{\rm eff}(r) = V(r) - \Omega^2 r^2/2 = (1-\Omega^2)r^2/2 + \lambda r^4/4$, the TF density profile can be approximated by

$$|\psi_{\rm TF}|^2 = \frac{\mu_{\rm TF} - V_{\rm eff}}{g} = \frac{1}{g}\left[\mu_{\rm TF} + \frac{\left(\Omega^2-1\right)r^2}{2} - \frac{\lambda r^4}{4}\right]. \tag{4}$$

For $\Omega < 1$, the TF density is maximum at the center ($r = 0$) and vanishes (cutoff) at $r = R \equiv [(\Omega^2-1) + \sqrt{4\lambda\mu_{\rm TF} + (\Omega^2-1)^2}]/\lambda$, where $\mu_{\rm TF}$ is defined positively. In contrast for $\Omega > 1$, it can be predicted from Eq. (4) that there could exist two radii where the TF density vanishes. They are

$$R^2_{\gtrless} = \frac{(\Omega^2-1) \pm \sqrt{4\lambda\mu_{\rm TF} + (\Omega^2-1)^2}}{\lambda}, \tag{5}$$

where $R_>$ (plus sign) corresponds to the outer radius, while $R_<$ (minus sign) corresponds to the inner radius. Moreover, for both $R_>$ and $R_<$ to be well defined (coexist), $\mu_{\rm TF}$ needs to be negative. In this case, the spatial extension of the atomic cloud is confined (cutoff) at $R_< \leqslant r \leqslant R_>$. By solving $\int_{R_<}^{R_>} 2\pi r dr\,|\psi_{\rm TF}|^2 = 1$, the negative chemical potential was found to be $\mu_{\rm TF} = (3g\sqrt{\lambda}/\pi)^{2/3}/4 - (\Omega^2-1)^2/(4\lambda)$. Accordingly, the system can be separated into two states demarcated by a critical rotating frequency Ω_c corresponding to $R_<(\Omega_c) = 0$ [or $\mu_{\rm TF}(\Omega_c) = 0$]. At sufficiently high rotating frequencies such that $\Omega > \Omega_c$ and hence $R_< > 0$, a central hole will appear in the condensates, i.e., in the VLH state [19,22]. In contrast for $\Omega < \Omega_c$, a vortex lattice without a central hole regime (the VL state) will appear. It is found that $\Omega_c^2 = 1 + (3\lambda^2 g/\pi)^{1/3}$, which is dependent of the interaction constant g and the quartic trap strength λ.

For the present binary-mixture condensates, the critical rotating frequency Ω_c, which characterizes the transition between the VL and the VLH states, can be qualitatively determined by the larger of g_{11} and g_{22}. As mentioned before, in this paper we consider only the cases $g_{11} \geqslant g_{22}$ (i.e., $\alpha_2 \leqslant 1$). Consequently,

$$\Omega_c^2 \equiv 1 + (3\lambda^2 g_{11}/\pi)^{\frac{1}{3}}. \tag{6}$$

When $\Omega < \Omega_c$, the rotating binary system will be in the VL state, while when $\Omega > \Omega_c$, the system will be in the VLH state. In the following subsection, two distinct cases of $g_{11} = 1300$ and $g_{11} = 55$ are studied. The former corresponds to the critical rotating frequency $\Omega_c = 3.43$ and hence $\Omega = 2.5 < \Omega_c$, while the latter corresponds to $\Omega_c = 2.18$ and hence $\Omega > \Omega_c$.

C. Vortex states

1. *VL state with $\Omega < \Omega_c$*

We first consider the vortex structures with rotation frequency below the critical rotating frequency, $\Omega < \Omega_c$. Figure 2 shows the equilibrium vortex structures of two-component condensates confined in a harmonic-plus-quartic potential with $g_{11} = g_{22} = 1300$ ($\alpha_2 = 1$) and $\alpha_{12} = 0.5$, 1, and 1.3 (from the top to the bottom) respectively. All three cases belong to the VL regime for which one is able to conclude the following. (i) For a phase-miscible mixture, the equilibrium state is composed of regular vortex lattices which form roughly a square lattice at $\alpha_{12} = 0.5$ rather than what is expected to be a triangular lattice when $\alpha_{12} \to 0$ [30] . (ii) At the isotropic point ($\alpha_2 = \alpha_{12} = 1$), a honeycomb lattice is formed for one component, while vortices in the other component form a vortex-pair lattice (the vortex of every pair has the same circulation). (iii) Stationary vortex sheets are formed for an asymmetric phase-separated mixture. Our results in Fig. 2 are intended to be compared to those shown in Figs. 2(a), 3, and 4 of Ref. [14]. With our results, we have been able to verify that the vortex structure shown in Fig. 3(b) of Ref. [14] corresponds to an authentic equilibrium state, while the one shown in Fig. 3(a) of Ref. [14] corresponds to a transition state.

Figure 3 shows the vortex structures of the mixtures with $g_{11} = 1300$, $\alpha_2 = 0.5$, and $\alpha_{12} = 0.8$. For these parameters, the system is still in the VL regime with $\Omega < \Omega_c$. In this case, the system has a ball-and-shell nonrotating ground state (phase III) and in the vortex state it forms an interlocking oniony vortex-sheet structure.

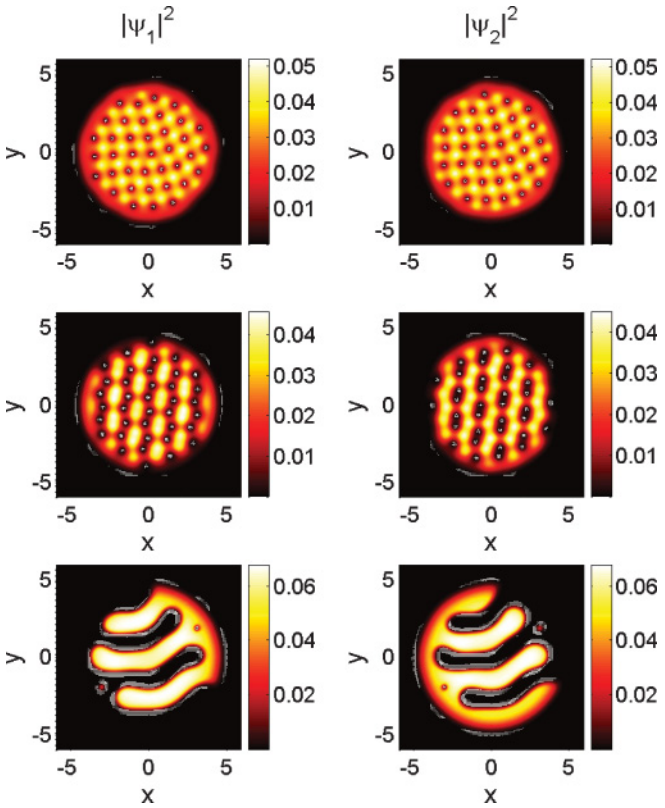

FIG. 2. (Color online) Vortex structures of fast-rotating binary-mixture condensates confined in a harmonic-plus-quartic potential in the VL state. The interaction constants $g_{11} = g_{22} = 1300$ ($\alpha_2 = 1$), the rotation rate $\Omega = 2.5$, and the quartic trap strength $\lambda = 1$ for all frames. From the top to the bottom rows, $\alpha_{12} = 0.7$, 1, and 1.3, respectively. x and y axes are in units of $\sqrt{\hbar/m\omega}$.

2. *VLH state with $\Omega > \Omega_c$*

The results in the VLH regime with $\Omega > \Omega_c$ are considered next. In this subsection, to see more clearly the vortex physics, we show the results of both the density profile $n_j(x,y) = |\psi_j(x,y)|^2$ and the phase profile given by

$$S_j(x,y) = \arctan\left[\frac{\mathrm{Im}\psi_j(x,y)}{\mathrm{Re}\psi_j(x,y)}\right]. \tag{7}$$

In the phase profile, the end point of the boundary between a π phase line and a $-\pi$ phase line will correspond to a vortex.

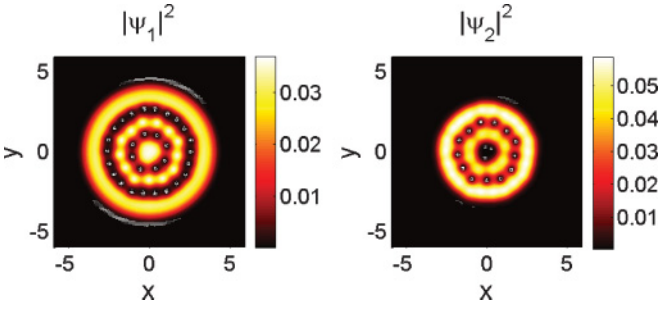

FIG. 3. (Color online) Vortex structures of components 1 (left panel) and 2 (right panel) in fast-rotating binary-mixture condensates in the VL state. Here $g_{11} = 1300$, $\alpha_2 = 0.5$, $\alpha_{12} = 0.8$, $\lambda = 1$, and $\Omega = 2.5$. x and y axes are in units of $\sqrt{\hbar/m\omega}$.

In addition, the circulation and the number of vortices can also be counted directly. Figure 4(a) shows the vortex structure and the corresponding phase profile of fast-rotating binary-mixture condensates with $g_{11} = 55, \alpha_2 = 1$, and $\alpha_{12} = 0.5$. The ground state of the corresponding nonrotating condensate mixture is miscible (phase I) to which the wave functions of the two components overlap entirely. In Fig. 4(a), it is found that the two annular vortex arrays interlock in a manner such that the density peak of one component is located at the density hole of the other component.

Figure 4(b) shows the vortex structure and the corresponding phase profile of the mixture with $g_{11} = 55$, $\alpha_2 = 1$, and $\alpha_{12} = 1.3$. The nonrotating counterpart has an asymmetric separated ground state (phase II in Fig. 1). Due to the strong repulsive interaction between two condensates which results in the asymmetric separated characteristic, the two condensates occupy the opposite side of each other.

Figure 4(c) shows the vortex structure and the corresponding phase profile of a condensate mixture with $g_{11} = 55$, $\alpha_2 = 0.5$, and $\alpha_{12} = 0.8$. With respect to phase III in Fig. 1, the nonrotating mixture has a ball-and-shell ground state, i.e., the component with the larger intraspecies interaction occupys the outside and forms a shell, while the component with the smaller intraspecies interaction occupys the inside and forms a ball. It is found that vortices in component 1 (of larger intraspecies interaction) form a circular array around the central low-density hole, while vortices in component 2 (of smaller intraspecies interaction) also form a circular array which is closer to the center (see the inset of the density profile or the phase profile plot). In addition to the vortices, the "ball" of the nonrotating counterpart of component 2 is actually pushed away (due to fast rotation) from the center and forms a robust ringlike condensate located where the vortices of component 1 are (i.e., interlocking). This robustness actually resists its own vortices revolving into it.

In Fig. 4(d), we also show the vortex structure and its corresponding phase profile of a mixture at the isotropic point, with $g_{11} = 55$ and $\alpha_2 = \alpha_{12} = 1$. Similar to the result of the middle row of Fig. 2, fast-rotating condensates tend to form the vortex-pair structure at the isotropic point.

D. Concluding remarks

The overall features of vortex structures in ultrafast-rotating binary-mixture condensates can be understood as follows. Pertaining to phase I in Fig. 1, when $\alpha_{12} = 0$ where the two components are not interacting with each other, the theory is essentially reduced to the one for single components. In this limit, triangular vortex lattices are expected to form with $\Omega < \Omega_c$, while annular vortex arrays are expected to form with $\Omega > \Omega_c$. As α_{12} is present and increases, vortex cores of one component gradually shift away from those of the other component and consequently with $\Omega < \Omega_c$ the triangular lattices are distorted. Eventually the vortices for each component will form a square lattice instead of a triangular one. As α_{12} exceeds α_2, equivalently for the system to shift to phase II or III, the condensates can undergo phase separation to spontaneously form domains. For one condensate, the cavity of another condensate is where the lower effective potential is, which is more apt to be occupied. However, more interlocking

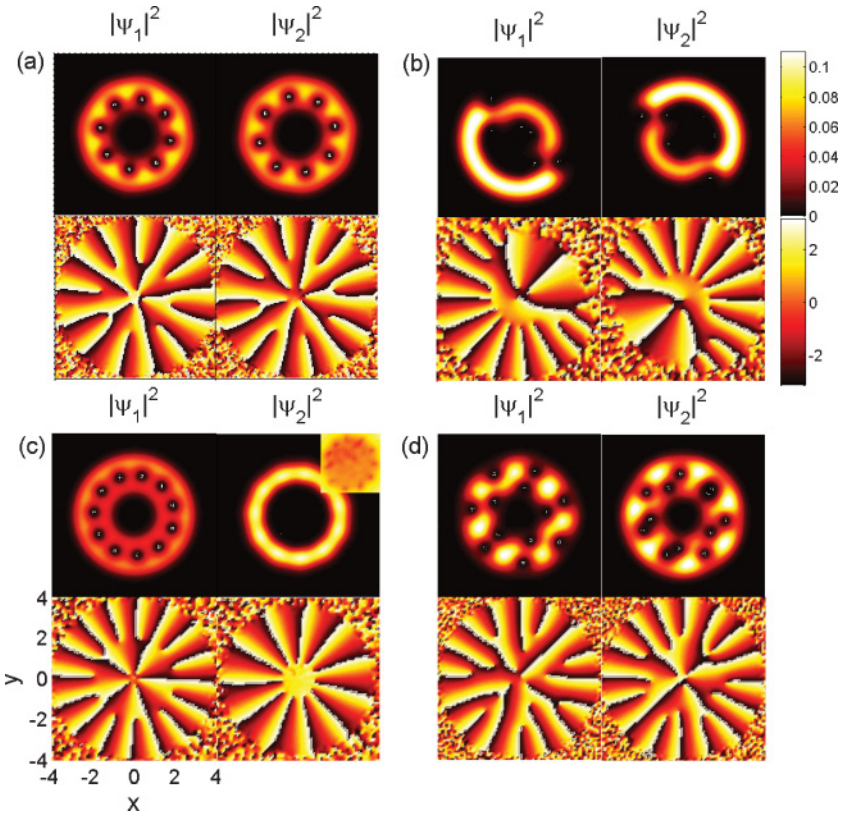

FIG. 4. (Color online) Vortex structures and phase profiles of ultrarapidly rotating binary-mixture condensates in the VLH state. In each panel, the top row (bottom row) corresponds to vortex structures (phase profiles), while the left column (right column) pertains to component 1 (2). Relative interactions are the following: (a) $\alpha_2 = 1$ and $\alpha_{12} = 0.5$, (b) $\alpha_2 = 1$ and $\alpha_{12} = 1.3$, (c) $\alpha_2 = 0.5$ and $\alpha_{12} = 0.8$, and (d) $\alpha_2 = 1$ and $\alpha_{12} = 1$. The interaction $g_{11} = 55$, quartic trap strength $\lambda = 1$, and rotation rate $\Omega = 2.5$ are fixed for all figures. The inset in panel (c) shows a more clear view of the vortices in component 2. x and y axes are in units of $\sqrt{\hbar/m\omega}$.

will cause wave functions to overlap more and at the same time raise the interspecies interaction energy $\propto g_{12}\,|\Psi_1|^2\,|\Psi_2|^2$. In order to prevent the above-mentioned interlocking that causes high energies, the vortices are actually concentrated out of the condensates and form the vortex sheets. Consequently the two components form structures complementary to each other and the total density is roughly described by the TF distribution $|\Psi_1|^2 + |\Psi_2|^2 \propto \max[\mu_{\rm TF} - (m\omega^2 r^2/2 + ur^4/4), 0]$. The results in the bottom row of Fig. 2 as well as in Figs. 3, 5, and 6 are examples of this.

IV. CONCLUSION

This paper investigates the equilibrium vortex structures of ultrafast-rotating binary-mixture condensates trapped in a harmonic-plus-quartic potential. In contrast to the harmonic trap alone case where the system is unstable when the rotation frequency Ω_0 is higher than the radial trap oscillator frequency ω, the added quartic trap can lead the system to remain stable at higher rotation velocity ($\Omega_0 > \omega$). Due to the complexity of interactions in the binary system, there often occur many metastable states in the fast-rotating two-component condensate system and the standard imaginary-time propagating approach may not really converge to the true equilibrium states of the system. In this regard, we have applied a combined numerical scheme to effectively assure that the density profiles do really saturate at sufficiently low temperatures. A critical rotating frequency Ω_c which characterizes the transition between the VL and the VLH states is identified. Under high-rotation frequencies ($\Omega_0 > \omega$), a variety of vortex structures of the two-component condensates are shown for $\Omega < \Omega_c$, similar to those presented in Ref. [14], and also for $\Omega > \Omega_c$ in particular for which various annular vortex structures occur.

ACKNOWLEDGMENTS

This work was supported by the National Science Council of Taiwan (Grants No. 99-2112-M-003-006-MY3, No. 98-2112-M-018-001-MY2, and No. 98-2115-M-035-001-MY2). We also acknowledge supports from the National Center for Theoretical Sciences (NCTS) and the Taida Institute for Mathematical Science (TIMS).

[1] M. R. Matthews, B. P. Anderson, P. C. Haljan, D. S. Hall, C. E. Wieman, and E. A. Cornell, Phys. Rev. Lett. **83**, 2498 (1999).
[2] J. R. Abo-Shaeer, C. Raman, J. M. Vogels, and W. Ketterle, Science **292**, 476 (2001).
[3] C. Raman, J. R. Abo-Shaeer, J. M. Vogels, K. Xu, and W. Ketterle, Phys. Rev. Lett. **87**, 210402 (2001).
[4] P. C. Haljan, I. Coddington, P. Engels, and E. A. Cornell, Phys. Rev. Lett. **87**, 210403 (2001).
[5] P. Engels, I. Coddington, P. C. Haljan, and E. A. Cornell, Phys. Rev. Lett. **89**, 100403 (2002).
[6] C. J. Myatt, E. A. Burt, R. W. Ghrist, E. A. Cornell, and C. E. Wieman, Phys. Rev. Lett. **78**, 586 (1997).

[7] B. D. Esry and C. H. Greene, Phys. Rev. A **59**, 1457 (1999).
[8] M. Trippenbach, K. Góral, K. Rzążewski, B. Malomed, and Y. B. Band, J. Phys. B **33**, 4017 (2000).
[9] F. Riboli and M. Modugno, Phys. Rev. A **65**, 063614 (2002).
[10] D. M. Jezek and P. Capuzzi, Phys. Rev. A **66**, 015602 (2002).
[11] A. A. Svidzinsky and S. T. Chui, Phys. Rev. A **67**, 053608 (2003).
[12] C. C. Huang and W. C. Wu, Phys. Rev. A **75**, 023609 (2007).
[13] E. J. Mueller and T. L. Ho, Phys. Rev. Lett. **88**, 180403 (2002).
[14] K. Kasamatsu, M. Tsubota, and M. Ueda, Phys. Rev. Lett. **91**, 150406 (2003).
[15] S. J. Woo, S. Choi, L. O. Baksmaty, and N. P. Bigelow, Phys. Rev. A **75**, 031604(R) (2007).
[16] E. Lundh, Phys. Rev. A **65**, 043604 (2002).
[17] K. Kasamatsu, M. Tsubota, and M. Ueda, Phys. Rev. A **66**, 053606 (2002).
[18] P. Engels, I. Coddington, P. C. Haljan, V. Schweikhard, and E. A. Cornell, Phys. Rev. Lett. **90**, 170405 (2003).
[19] G. M. Kavoulakis and G. Baym, New J. Phys. **5**, 51 (2003).
[20] V. Bretin, S. Stock, Y. Seurin, and J. Dalibard, Phys. Rev. Lett. **92**, 050403 (2004).
[21] T. P. Simula, A. A. Penckwitt, and R. J. Ballagh, Phys. Rev. Lett. **92**, 060401 (2004).
[22] A. L. Fetter, B. Jackson, and S. Stringari, Phys. Rev. A **71**, 013605 (2005).
[23] C. C. Huang, C. H. Liu, and W. C. Wu, Phys. Rev. A **81**, 043605 (2010).
[24] S. Choi, S. A. Morgan, and K. Burnett, Phys. Rev. A **57**, 4057 (1998).
[25] H. T. C. Stoof, J. Low Temp. Phys. **114**, 11 (1999).
[26] H. T. C. Stoof, J. Low Temp. Phys. **124**, 431 (2001).
[27] C. W. Gardiner, J. R. Anglin, and T. I. A. Fudge, J. Phys. B **35**, 1555 (2002).
[28] C. W. Gardiner and M. J. Davis, J. Phys. B **36**, 4731 (2003).
[29] A. S. Bradley, C. W. Gardiner, and M. J. Davis, Phys. Rev. A **77**, 033616 (2008).
[30] As discussed in Ref. [14], interaction energy $E_{\rm int}$ can be expressed in terms of the total density $n = |\Psi_1|^2 + |\Psi_2|^2$ and the spin variable $S = |\Psi_1|^2 - |\Psi_2|^2$ as $E_{\rm int} = (C_{11}/8) \int d\mathbf{r}[(1+\alpha_2+2\alpha_{12})\, n^2 + (1+\alpha_2-2\alpha_{12})\, S^2 + 2\,(1-\alpha_2)\, nS]$. If the coefficient $(1+\alpha_2-2\alpha_{12})$ is positive, antiferromagnetism manifests and makes a square lattice stabilized.